Radiation Physics and Chemistry 156 (2019) 58–66

Contents lists available at ScienceDirect

Radiation Physics and Chemistry

journal homepage: www.elsevier.com/locate/radphyschem

Amine functionalized radiation induced grafted polyolefin nanofibers for CO_2 adsorption

Ali Abbasi[a], Mohamed Mahmoud Nasef[b], Soorathep Kheawhom[a,*], Reza Faridi-Majidi[c], Matsuura Takeshi[d], Ebrahim Abouzari-Lotf[e,f], Thomas Choong[g]

[a] Computational Process Engineering Research Laboratory, Department of Chemical Engineering, Faculty of Engineering, Chulalongkorn University, Bangkok 10330, Thailand
[b] Chemical Engineering Department, Universiti Teknologi PETRONAS, Bandar, Seri Iskandar, 32610 Perak, Malaysia
[c] Department of Medical Nanotechnology, School of Advanced Technologies in Medicine, Tehran University of Medical Sciences, Tehran, Iran
[d] Department of Chemical & Biological Engineering, University of Ottawa, Ottawa, ON, Canada K1N 6N5
[e] Faculty of Chemical and Energy Engineering, Universiti Teknologi Malaysia, 81310 Johor Bahru, Malaysia
[f] Advanced Materials Research Group, Center of Hydrogen Energy, Institute of Future Energy, Universiti Teknologi Malaysia, 54100 Kuala Lumpur, Malaysia
[g] Department of Chemical and Environmental Engineering, Universiti Putra Malaysia, 43400 Selangor, Malaysia

ARTICLE INFO

Keywords:
CO_2 adsorption
Solid supported adsorbent
Radiation induced grafting
Nanofibers
Glycidyl methacrylate

ABSTRACT

A new type of nanofibrous amine-containing adsorbent was prepared for CO_2 adsorption by electrospinning of syndiotactic polypropylene (s-PP) followed by radiation induced grafting of glycidyl methacrylate and subsequent amination with ethanolamine. The obtained adsorbents were tested for CO_2 adsorption with a mixture of CO_2/N_2 having 5–15% CO_2 using a fixed bed adsorption column at atmospheric pressure. A maximum adsorption capacity of 2.87 mmol/g was achieved for the sample with degree of grafting of 300% and degree of amination of 94% at feed concentration of 15% at 30 °C. This was accompanied by good mechanical characteristics and a very high amine efficiency that reached 75% at room temperature, suggesting that the obtained fibrous adsorbent has high potential for CO_2 adsorption.

1. Introduction

CO_2 is the most critical greenhouse gas released into the atmosphere in large quantities. This large amount of CO_2 causes global warming and its natural disastrous consequences. The main contribution (~85%) of the CO_2 emission comes from the combustion of fossil fuels which are the main source for meeting energy demands (IEA, 2015). Currently, liquid amine absorption (also known as amine scrubbing) is the main commercial method used for CO_2 capturing. This method involves the use of monoethanolamine (EA), diethanolamine, or methyldiethanolamine solutions for CO_2 removal (Kuenemann and Fourches, 2017). However, the process involves a number of serious challenges including high regeneration energy, large equipment size, amine degradation, and equipment corrosion (Rochelle, 2009).

Recently, there has been a great interest on solid adsorbents, especially chemisorbents, for CO_2 capture. Chemi-sorbents usually contain amine functional groups, immobilized on organic or hybrid solid substrates using physical or chemical interactions. However, physically impregnated amines on organic substrates are challenged by amine leaching after few adsorption/desorption cycles (Parvazinia et al., 2018). Unlike physisorbents, covalent bonding of amine-containing group to the substrate gives chemisorbents high adsorption capacity and more stability, but adversely affects the amine efficiency and adsorption kinetics.

Among solid adsorbents containing amine functional groups (Hosseini et al., 2015), microfibers and microporous polymers have shown some advantages over other adsorbents using different substrates. Particularly, fibrous adsorbents have flexibility, low pressure drop, and short transit distance (Zhuang et al., 2013; Rojek et al., 2017). However, the adsorption capacity of these adsorbents is relatively low because of incomplete access to amine functional groups. Moreover, the work capacity and production cost of the adsorbent are issues requiring further development. Reducing the fibers' size from micro-scale to nano-scale is an interesting approach that could improve the work capacity and the efficiency of fibrous adsorbents. The nanofibrous mats have the advantages of high surface area and weight to volume ratio in addition to having 3-D structure with porous interconnected architecture. Although there are many ways for producing

* Corresponding author.
E-mail address: soorathep.k@chula.ac.th (S. Kheawhom).

https://doi.org/10.1016/j.radphyschem.2018.10.015
Received 14 August 2018; Received in revised form 16 October 2018; Accepted 19 October 2018
Available online 26 October 2018
0969-806X/

nanofibers, such as phase separation (Zhang et al., 2017) and template synthesis (Costa et al., 2017), electrospinning is the most versatile and commonly used method (Abbasi et al., 2014).

There have been some reports using electrospun nanofibrous structures for CO_2 capture. Typically, polyacrylonitrile (PAN) electrospun nanofibers were used as the support for Cu-based metal organic framework which are known for their large surface area and high adsorption and storage capacity for CO_2 gas (Wahiduzzaman et al., 2015). In another study, polyamide-6/amine-functionalized carbon nanotube composite nanofibrous mats were impregnated with polyethyleneimine (PEI) to increase its capacity and selectivity toward CO_2. The prepared materials showed maximum adsorption capacity of 1.16 mmol CO_2 per gram of the adsorbent, comparable to other organic polymer-based CO_2 adsorbents (Zainab et al., 2017). More recently, PAN was functionalized using various amines to incorporate required functionality for efficient transport of humid CO_2. The study showed that CO_2 capture capability of the PAN nanofibers increased with chemical modification using amines due to the change in chemical and morphological structure of the fibers (Olivieri et al., 2018).

To utilize nanofibers as promising materials for adsorbent applications, they usually need to be modified with various techniques to impart functional or ionic groups and desired characteristics. These methods include dip-coating, interfacial polymerization, and radiation induced grafting (RIG). Of all, RIG is promising modification technique because of its potency to permanently modify polymeric substrates in various physical forms (films, particles or fibers) without changing their inherent properties (Nasef et al., 2016). Therefore, combining these two fascinating techniques (electrospinning and RIG) could provide a versatile and convenient way for producing polymeric nanofibrous adsorbent for CO_2.

The objective of this study is to develop a new nanofibrous amine containing adsorbent for CO_2 removal from different environments at ambient conditions using electrospinning of s-PP followed by RIG of GMA and subsequent functionalization with EA. Using low cost starting materials and simple and flexible preparation procedure makes these adsorbents interesting candidates to be used for CO_2 removal.

2. Experimental

2.1. Materials

s-PP (M_w = 174,000; M_n = 75,000), decahydronaphthalene (decalin) (reagent grade, 98%), dimethylformamide (DMF, ≥ 99.8%), GMA (purity ≥ 99%), EA (purity ≥ 99%), and tetrahydrofuran (THF) (anhydrous, ≥ 99.9%) were purchased from Sigma-Aldrich. Acetone (Analytical grade, Fischer Scientific) and methanol (Merck Millipore) were used as received without further purification. CO_2 and N_2 gas (> 99.99%) were supplied by Linde AG (Malaysia). Deionized (DI) water was used for washing and preparation of solutions.

2.2. Preparation of adsorbents

2.2.1. Electrospinning of s-PP

s-PP nanofibrous substrates with specific surface area of above 2.0 m^2/g were prepared by electrospinning of 7.5 wt/v% solution in a mixture of decalin, acetone and DMF (80:10:10 wt%) under optimum conditions using an automated electrospinning machine (Electroris, FNM Co. Ltd, Iran) as reported elsewhere (Abbasi et al., 2018; Abouzari-lotf et al., 2017). The obtained nanofibrous substrates were dried at 60 °C in an oven for 24 h to remove all residual solvents.

2.2.2. Graft polymerization of GMA onto s-PP electrospun substrates

Pre-irradiation technique was used to graft GMA onto the electrospun s-PP nanofibrous substrates. The sheets with the size of 4 × 4 cm were irradiated under vacuum in sealed polyethylene plastic bags on dry ice using a universal electron beam accelerator (NHV—Nissin High Voltage, EPS3000, Cockroft Walton type, Japan). The accelerator was operated with an acceleration voltage of 1 MeV and a beam current of 10 mA with a total dose in the range of 40–200 kGy. Irradiation was carried out under vacuum to prevent the reaction of free radicals formed on the polymer chains with oxygen molecules in air and formation of peroxides and hydroperoxides. Dry ice was used to stabilize radicals formed in the nanofibers during irradiation and prevent any possible damage to the samples because of temperature increase. After irradiation, the samples were kept inside a freezer at −40 °C to stabilize formed radicals on the polymer backbone before being used in the grafting reaction within 3 days.

GMA solution in methanol with the concentration in a range from 2.5 to 20 vol% was purged with pure nitrogen. The oxygen-free solution was then transferred to an evacuated ampoule containing irradiated nanofibers and flushed with nitrogen gas for another 5 min. The ampoule was then sealed and heated for 20–120 min in a temperature range of 40–70 °C in an oven. The grafted samples were rinsed several times with methanol to remove any un-reacted monomers, followed by shaking in pure THF for 12 h to eliminate any formed homopolymers from the grafted sheets. The purified sample then was dried in a vacuum oven at 60 °C and weighed (W_g) to obtain the degree of grafting (DG). DG was calculated by Eq. (1) (Abbasi et al., 2018).

$$DG(\%) = \frac{W_g - W_0}{W_0} \times 100 \quad (1)$$

Where, W_g and W_o are the weights of the sample before and after grafting, respectively.

2.2.3. Amination of poly(GMA)-grafted substrates

A sample of poly(GMA)-grafted s-PP substrate was immersed in a solution of EA with concentrations in the range of 20–100% (v/v) in water and stirred at temperatures in the range of 30–80 °C under reflux condition for different time intervals in the range of 7–240 min. After reaction completion, the sample was removed and washed with DI water several times to remove all un-reacted amines. Then, it was dried at 60 °C in a vacuum oven for 2 h and weighted to calculate the degree of amination (DA) using Eq. (2) (Choi et al., 1999).

$$DA(\%) = \frac{(W_a - W_g)/61.08}{(W_g - W_0)/142.15} \times 100 \quad (2)$$

where, W_a, W_g and W_0 are the weights of the sample after amination, after grafting and before grafting, respectively. The figures of 61.08 and 142.15 in Eq. (2) are the molecular weights of EA and GMA, respectively. A schematic view of the experimental setup used for radiation induced grafting reactions could be found in Fig. S1 (Supplementary documents).

2.2.4. CO_2 adsorption tests

A fixed-bed column CO_2 adsorption system developed by Solutions Sdn. Bhd.(Malaysia) was used to test CO_2 adsorption capacity of the prepared samples under dynamic conditions. The column is made of stainless steel with a height of 330 mm and internal diameter of 250 mm. There was a porous ceramic monolith with a height of 30 mm located at the bottom of the column to hold the adsorbent samples. The temperature was controlled by a heating element coiled around the column in connection with two K-type thermocouples with an accuracy of ± 1.5 °C located at the height of 75 mm and 280 mm from the column base to monitor the inlet and outlet gas temperature.

The adsorption tests were carried out at atmospheric pressure with a mixture of CO_2/N_2 gases with total flow rate of 50 ml/min having CO_2 concentration ranging from 5 to 15 vol%. Two mass flow controllers (GFC series, Dwyer Instruments) were used to accurately control the flow of CO_2 and N_2 in the range of 1–50 and 1–100 ml/min, respectively. The accuracy and repeatability of the flow controllers was ± 1.5% and ± 0.5% of the full scale. A CO_2 analyzer (GfG Gesellschaft für

Gerätebau IR 24) with a maximum detection limit of 50 vol% was used to monitor the CO_2 concentration before and after adsorption. The nitrogen gas was humidified by going through a water bubbler at 60 °C to introduce humidity to the stream and then mixed with CO_2. The relative humidity of the gas stream was about 80% as determined by Fisher-Scientific lab hygrometer.

The dynamic adsorption capacity of the samples was calculated using Eq. (3) (Serna-Guerrero and Sayari, 2010).

$$q = \frac{F \times C_0 \times t_q}{W} \tag{3}$$

where, F is total flow rate (mmol/s), C_0 is the initial concentration of CO_2, W is the weight of the adsorbent (g) and t_q is the stoichiometric time (s) which is calculated using the breakthrough curve according to the Eq. (4) (Serna-Guerrero and Sayari, 2010).

$$t_q = \int_0^\infty \left(1 - \frac{C}{C_0}\right) dt \tag{4}$$

where, C and C_0 are the concentrations of CO_2 at the inlet and the outlet gas streams, respectively. A schematic diagram of the fixed bed CO_2 adsorption system and the details on the adsorption experiments could be found in the Supplementary document (Fig. S2).

Amine efficiency is defined as the ratio of the moles of CO_2 molecules adsorbed on the material to the moles of nitrogen atoms available on the sample (Drese, 2010). The maximum amine efficiency of an adsorbent depends on the amine type and the presence or absence of water molecules. The maximum amine efficiency of primary amines in humid conditions which was sued in these experiments is 1. So, for the calculation of amine efficiency, the following equation was used:

$$\text{Amine efficiency}(\%) = (\text{q/amine density}) x 100 \tag{5}$$

where, q is the adsorption capacity and amine density is the moles of the amine functional groups per gram of the adsorbent.

The effect of temperature, initial CO_2 concentration and the degree of grafting (amine density) on the adsorption capacity was investigated. Temperature was changed in the range of 30–50 °C. Samples with various DGs in the range of 150–400% were used. The initial concentration of CO_2 was changed in the range of 5–15%.

Regeneration of the adsorbents was completed by changing the flow to 100 ml/min pure N_2 and increasing the temperature to 80 °C for 15 min. At the same time, CO_2 concentration in the outlet stream was monitored to make sure of removing all the adsorbed molecules form the adsorbent.

2.3. Characterization

The morphology of the final adsorbents and their corresponding precursors was studied using a Hitachi S3400N scanning electron microscope (SEM) with an acceleration voltage of 10 kV and magnification of 1000–5000× after coating with gold. The diameters of 30 random fibers of each sample were measured and used to estimate the average fiber diameter. The thickness of the prepared substrates was measured using a Pro'sKit digital caliper (Model: 400-044). Chemical changes in the samples were investigated using a Nexus 670 Thermo Nicolet FTIR in the frequency range of 4000–400 cm^{-1} with a resolution of 4 cm^{-1} and 5-time scans.

Differential scanning calorimetry (DSC) were carried out with a Q200 TA Instrument to study the melting temperature of the prepared samples. 5–10 mg of each sample was heated under nitrogen atmosphere (flow rate: 50 ml min^{-1}) in the heating range of 30–300 °C with a heating rate of 10 °C min^{-1}. Thermogravimetric analysis (TGA) was performed using a Mettler Toledo TGA/SDTA 851e unit in the temperature range of 30–600 °C at a heating rate of 10 °C min^{-1}.

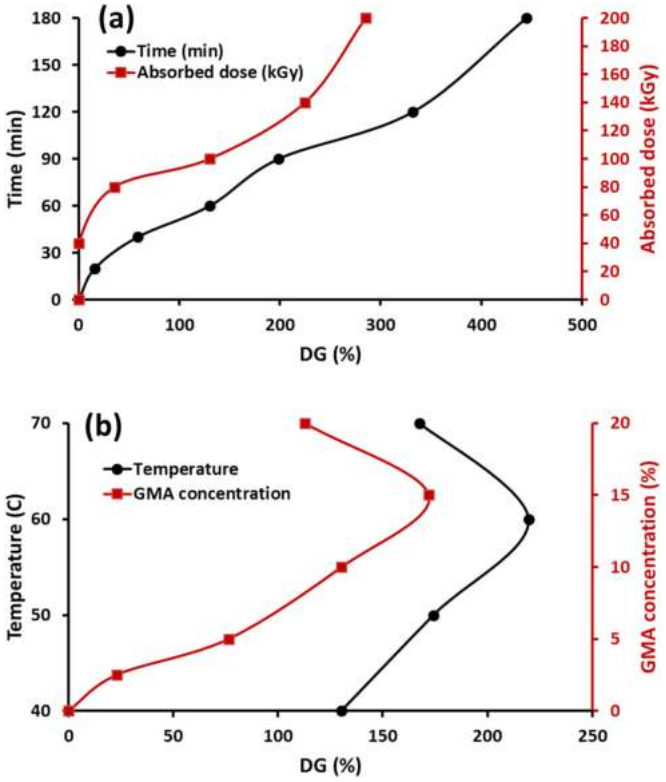

Fig. 1. Effect of (a) time and absorbed dose and (b) temperature and monomer concentration on the DG of GMA.

3. Results and discussion

3.1. Electrospinning

The electrospinning conditions such as applied voltage, needle tip to collector distance (TCD), and flow rate (considered as independent parameters) were varied according to the combinations obtained by Box-Behnken design (BBD) of RSM. The results of this optimization and modeling has already been reported in our previous publication (Abbasi et al., 2018). Electrospun nanofibers with average fiber diameter of 439 nm were selected to be used in the rest of this study, because of their proper production rate and good fiber quality.

3.2. Effect of grafting parameters

The effect of various grafting parameters on the degree of grafting are depicted in Fig. 1. To study the effect of absorbed dose, other parameters including grafting time, grafting temperature and monomer concentration were set at 60 min, 40 °C and 10 vol% and the dose was changed from 40 to 200 kGy (Fig. 1a). Up to a dose of 40 kGy, no measurable grafting reaction was observed, most likely due to lack of sufficient stable radicals in nanofibrous s-PP substrate. With increasing the absorbed dose to 80 kGy and above, the DG increased gradually from 35% to 285%, showing that with higher absorbed dose more radicals are formed on the fibers, providing more sites for grafting reaction. Fig. 1a also shows the effect of grafting time on the DG with absorbed dose, monomer concentration and grafting temperature set at 100 kGy, 10 vol% and 40 °C, respectively. The DG increased with the increase in the grafting time in the investigated time, reaching 445% for 180 min. The increase in the grafting time allowed not only initiation of grafting with more activated radicals but also more propagation to longer graft polymer chains.

The effect of temperature and monomer concentration on the DG is shown in Fig. 1b. For monomer concentration study, grafting

parameters including absorbed dose, grafting time and temperature were set at 100 kGy, 60 min and 40 °C, respectively. With increasing the monomer concentration in the range of 2.5–15 vol%, the DG increased as well. Further increase in the monomer concentration to 20 vol% resulted in a remarkable drop in the DG. The appearance of maximum DG in the diluted monomer solution could be explained by Trommsdorff effect which has been explained in details in a number of earlier studies (Choi and Nho, 1999).

While studying the effect of grafting temperature, other reaction parameters including absorbed dose, monomer concentration and grafting time were set at 100 kGy, 10 vol% and 60 min, respectively. Increase reaction temperature from 40° to 60°C resulted in a considerable increase in the DG from 130% to 220%. This is due to the increase in activation of radicals and the rate of monomer diffusion leading to significant rise in their involvement in the grafting reaction. Further increase in the reaction temperature up to 70 °C lead to a decrease in the DG due to the recombination of some radicals and termination of some graft growing chains by recombination (Nasef and Hegazy, 2004). These results show that the degree of grafting depends strongly upon the grafting parameters.

3.3. Effect of amination parameters

Fig. 2a shows the effect of reaction time variation on the DA of samples with various DGs. Reaction temperature and amine concentration were set at 60 °C and 50 vol% in water, respectively. As could be seen, the DA increased for three samples with various DGs (150%, 300% and 400%) with the increase in the reaction time but the increase was very sharp in the first 30 min followed by a very slight increase up to 120 min beyond which it reached to a plateau and DA achieved saturation. The trend was the same for samples with various DGs.

It can be clearly seen that higher DA was achieved with lower DG.

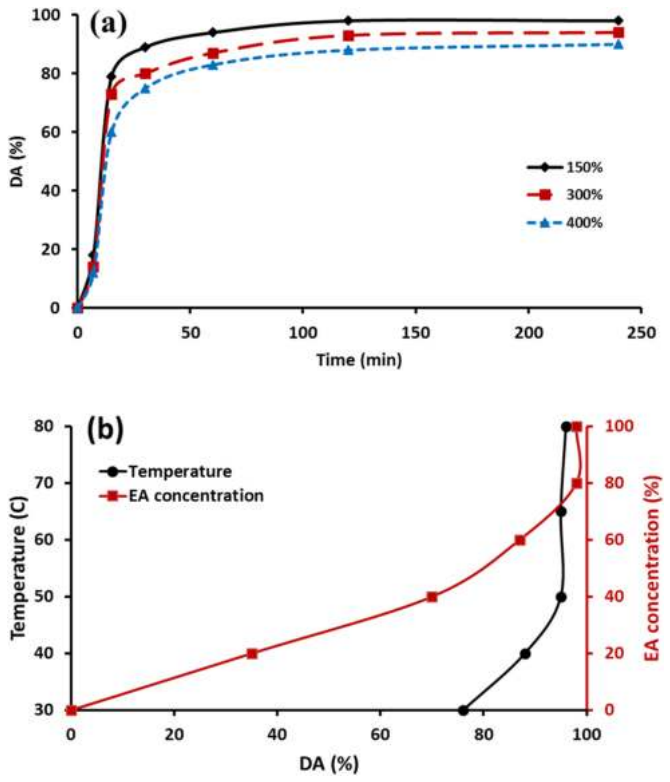

Fig. 2. Effect of (a) reaction time (T = 60 °C, C = 60%), (b) reaction temperature (t = 60 min and C = 50%), and EA concentration (t = 60 min and T = 60 °C) on the DA of poly(GMA) grafted s-PP samples.

For the sample with the DG of 150%, a maximum DA obtained after 240 min was 98%, while the corresponding values for the samples with 300% and 400% DGs decreased to 94% and 90%, respectively. This could be attributed to the decrease in the pore sizes available in the samples, which obscure the access to epoxy groups required for amination with increasing the DG. This means less diffusion of the amination solution occurred into the fibrous mat and hence, lower DA was achieved during the same time.

The effect of temperature and EA concentration on the DA can be seen in Fig. 2b. The DA increased sharply with increasing reaction temperature from 76% at 30 °C to 95% at 50 °C beyond which it reached to a plateau. This reveals that the increase of the temperature to 50 °C not only facilitated the diffusion of the amine solution into the nanofibrous mat, but also prompted in the ring opening reaction of the epoxy originated from Poly-GMA side chains (Zhuang et al., 2013). Further increase in the temperature did not have significant effect on the DA and therefore, optimum temperature for doing the amination reaction was maintained 50 °C. Moreover, the EA concentration variation from 20% to 100% in water lead to an increase in DA from 35% to 98%. This could be ascribed to the increase in the frequency of efficient collisions between amine molecules and epoxy groups due to increased concentration of the amine molecules in water.

3.4. Morphology of electrospun nanofibers

Fig. 3 shows SEM images of s-PP nanofibers in different stages of preparation. The average fiber diameter increased from 439 ± 173 nm to 482 ± 175 nm after grafting and more beads were formed in the electrospun sample (c, d) (Abbasi et al., 2018). The average fiber diameter of nanofibers also increased with an increase in DA. It increased from 482 ± 175 nm for grafted samples to 679 ± 233 nm, 730 ± 195 nm and 774 ± 219 nm for the aminated samples with DA of 30%, 60% and 94%, respectively (e to j). This diameter increase can be attributed to the layer of amine groups wrapping the grafted s-PP nanofibers (Zhuang et al., 2013). The thickness of the electrospun nanofibers also increased from about 50 μm for pristine s-PP nanofibers to 140, 210, and 260 μm after grafting with GMA by 150%, 300% and 400%, respectively. After amination using EA no considerable thickness change was observed in the substrates. Besides, the fibers morphology also changed, and more twisted fibers were observed with the increase in DA. For instance, most of the fibers were twisted around each other, making helix-like structures in the sample, as can be seen in Fig. 3i and j. This could be ascribed to the higher interaction between fibers due to the introduction of amine and hydroxyl functional groups and the presence of hydrogen bonding between the aminated fibers. This effect has already been reported for materials aminated from other amination agents (Almasian et al., 2016). Moreover, the adsorbent with 300% DG and 94% DA showed reasonable mechanical properties as the tensile strength of 18 ± 2 MPa and elongation at break of 53 ± 5% was recorded. Such good mechanical integrity could be attributed to the presence of hydrogen bonding in the adsorbent structure along inherent mechanical characteristics of PP.

3.5. Chemical changes

Introduction of GMA onto electrospun s-PP nanofibers and subsequent modification with EA was confirmed by FTIR spectroscopy. As could be seen in Fig. 4, new absorption bands at 1725, 1255, 905 and 845 cm^{-1} appeared after grafting. The strong band at 1725 cm^{-1} and the weak broad band at 1255 cm^{-1} are characteristics for -C=O and C-O- stretching of acrylate, respectively (Choi et al., 2001). The two small peaks at 905 and 845 cm^{-1} are attributed to the epoxy ring (Zhuang et al., 2013; Nasef et al., 2014; Bondar et al., 2004). The characteristic intensity of the carbonyl band of poly(GMA) side chains at 1725 cm^{-1} did not change during the amination reaction. However, with increasing the DA from 30% (c) to 60% (d) and then to 94% (e), the

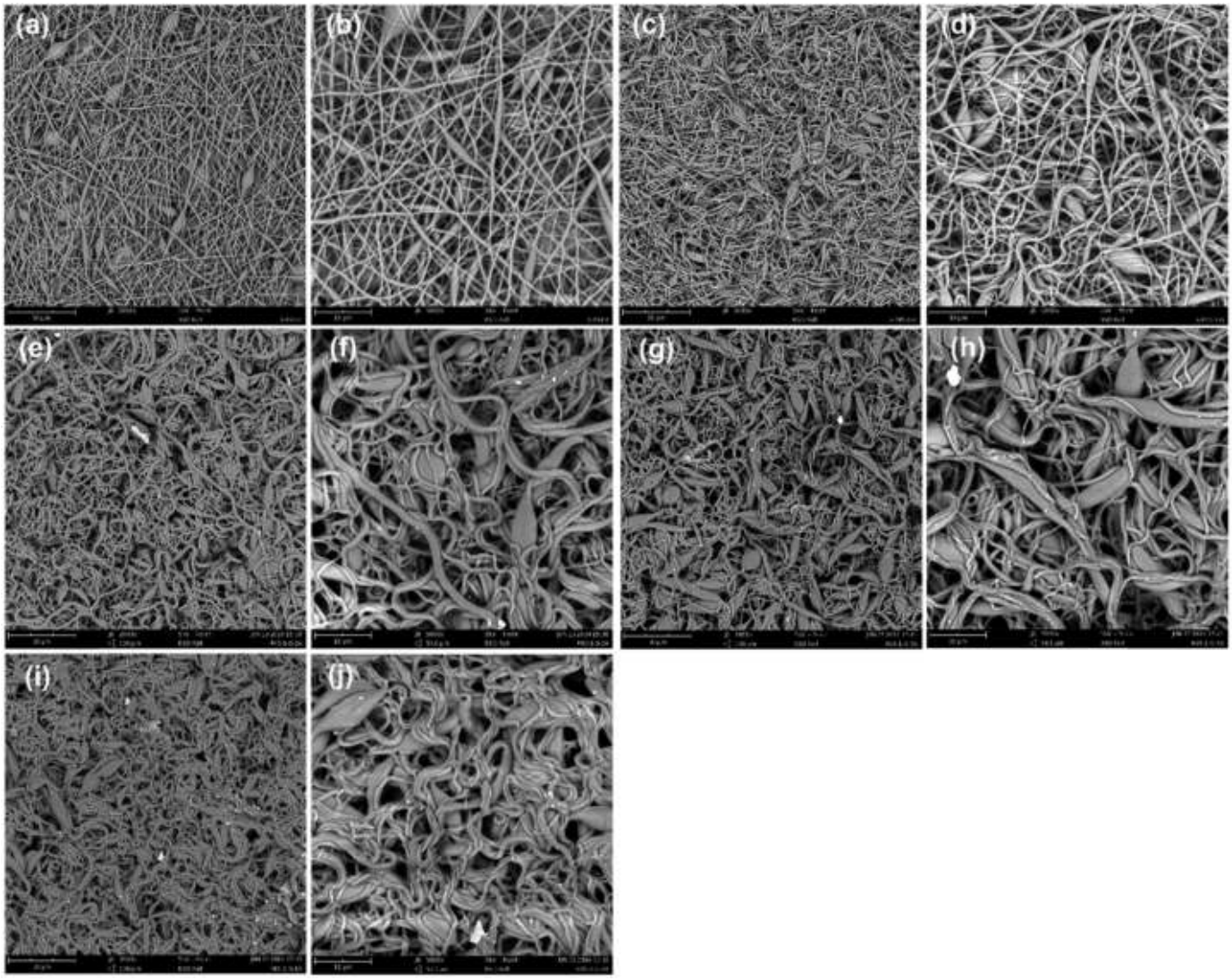

Fig. 3. SEM images of pristine s-PP nanofibers (a, b) 150% poly(GMA)-grafted nanofibers (c, d) and nanofibers aminated with EA with DA of 30% (e, f), 60% (g, h) and 94% (i,j).

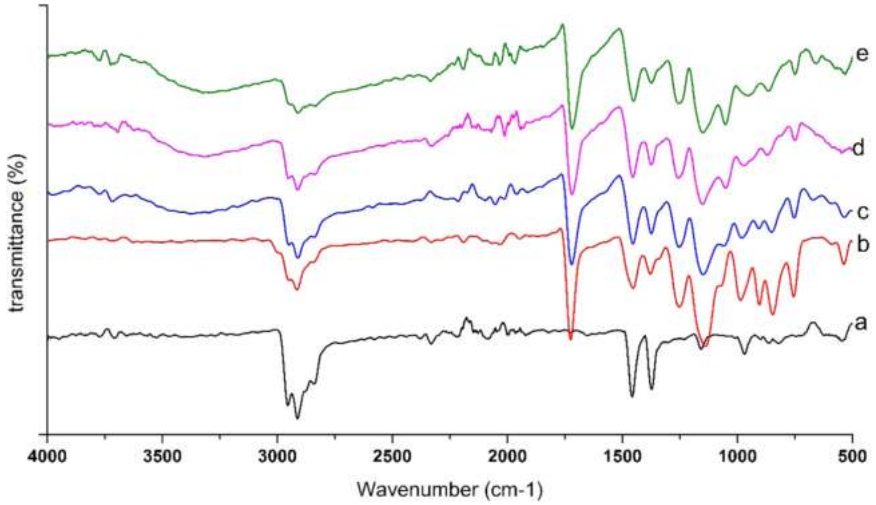

Fig. 4. FTIR spectra of pristine s-PP nanofibers (a) compared with 300% grafted nanofibers (b) and fibers with 30% (c), 60% (d) and 94% (e) DA using EA.

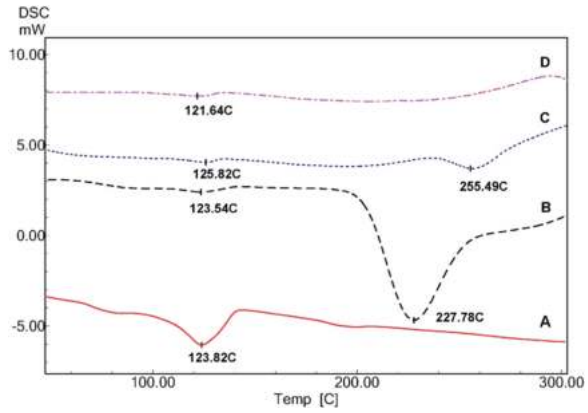

Fig. 5. DSC thermograms of pristine nanofibers (A), 300% GMA grafted nanofibers (B) and EA aminated nanofibers with 30% (C) and 94% (DC) DA.

intensity of the bands at 905 and 845 cm^{-1} related to epoxy group of poly(GMA) side chains, decreased so that for 94% these peaks almost disappeared. Furthermore, a new broad band at 3500–3000 cm^{-1} was appeared, which is due to O-H stretch of hydroxyl group at about 3400 cm^{-1}, overlapping with N-H stretch of secondary amine group at about 3300 cm^{-1} (Zhuang et al., 2013). C-N stretching vibration of aliphatic amines appears at 1250–1020 cm^{-1}. However, this area of the spectrum is loaded with several characteristic peaks of the s-PP base polymer and the C-N peak was obscured. These results agree with SEM images and further confirm the successful amination of the grafted samples that was accompanied the opening of epoxy rings of grafted poly (GMA).

3.6. Thermal properties

Fig. 5 shows DSC thermograms of pristine, poly(GMA)-grafted and EA-aminated nanofibers with various DAs. The endothermic peak at about 124 °C is for the melting temperature of pristine s-PP, which became very weak and shifted for grafted and aminated samples. The grafted nanofibers showed an additional broad peak at 227 °C due to the first stage decomposition of poly(GMA) side chains. For 30% aminated sample, a small peak was observed at 255 °C and for 94% DA, no peak was seen for temperatures up to 300 °C.

TGA thermograms of pristine s-PP nanofibers shows a single step degradation at 460.75 °C, attributed to the main polymeric backbone thermal decomposition (Fig. 6). After grafting, a 3-stage decomposition behavior at 228, 313 and 455 °C was observed. The first and second decomposition stages are related to the decomposition of glycidyl and carboxyl groups of GMA side chains, respectively (Choi et al., 2001). The final decomposition stage is for thermal decomposition of the main s-PP backbone, similar to the pristine s-PP nanofibers. After 30% amination with EA, a 4-stage decomposition pattern was observed. The first

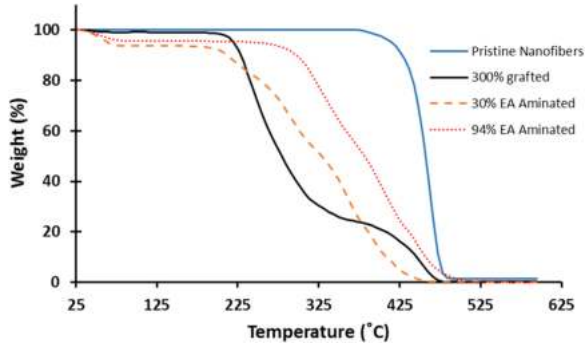

Fig. 6. TGA of pristine, poly(GMA) grafted and EA aminated s-PP nanofibers with various DAs.

weight loss was due to the moisture adsorbed on the aminated samples, showing hydrophilic nature of the mats after amination (Choi et al., 2001). Two decomposition peaks of GMA side chains became smaller and moved to 251 and 336 °C. A totally new peak appeared at 420 °C and decomposition peak of polymeric backbone appeared at 465 °C. The peak at 420 °C could be attributed to the aminated species. Further amination up to 94% led to the disappearance of the peak at 251 °C and a 3-stage decomposition was observed for this sample. This peak was related to the decomposition of poly(GMA) in the grafted polymer, as discussed before. The disappearance of this peak confirms successful amination reaction.

Amination of poly(GMA)-grafted s-PP nanofibrous with DG of 300% using EA to 30% improved the thermal stability of the nanofibrous structure. Degradation started at almost the same temperature of 200 °C. However, because of the opening of some of the unstable epoxy rings due to amination reaction, the thermal stability showed some improvement. This ring opening reaction removes the stress of the three-membered epoxy ring and improves sample's stability. Increasing the DA to 94% led to a further improvement in the thermal stability and degradation started at higher temperature of about 300 °C. This stability could be attributed to the opening of most of epoxy rings.

3.7. CO_2 adsorption

The breakthrough curves of CO_2 adsorption on s-PP nanofibers grafted by GMA and aminated using EA are presented in Fig. 7. To study the effect of temperature, adsorption was carried out using three different temperatures, i.e. 30, 40 and 50 °C. Fig. 7A shows that with increasing the adsorption temperature, the breakthrough curve was shifted to the left (shorter times) and the adsorption capacity decreased from 2.57 to 1.67 and 1.04 mmol CO_2/g of the adsorbent, respectively. This agrees very well with thermodynamic of the adsorption. Since both the entropy change and the heat of adsorption are negative for the adsorption of CO_2 on amines, the increase in the temperature decreases the adsorption capacity. This trend is in a complete agreement with previous studies (Drese, 2010).

Table 1 summarizes the adsorption capacities of nanofibrous s-PP adsorbents grafted by poly(GMA) and aminated using EA.

To study the effect of the DG and hence, amine density on the CO_2 adsorption capacity, three samples with various DGs with maximum DA obtained for each sample was used. Fig. 7B reveals the breakthrough curve for CO_2 adsorption on adsorbents with different DGs and amine densities using the same adsorption conditions. With increasing the DG, the number of epoxy rings on the sample, ready to react with the amine group were increased. Therefore, it is expected to have higher amine density for higher DG and hence, higher adsorption capacity. However, as could be seen in Table 1, with increase in the DG in the order of 150%, 300% and 400%, the highest DA decreased from 98 to 94 and 90, respectively. This was accompanied by a rise in the amine density of the samples in the sequence of 3.30, 3.81 and 3.87 mmol/g, for the samples with DGs of 150%, 300% and 400%, respectively.

Amine efficiency for the EA-aminated samples with the DG of 150%, 300% and 400% shown in Table 1 was 68.5%, 67.5% and 59%, respectively. Combining amine density and amine efficiency of a sample defines its adsorption capacity. For the adsorbents containing EA, the sample with the DG of 300% showed the highest adsorption capacity (q) of 2.57 mmol CO_2/g of the adsorbent compared to 150% and 400% in which q of 2.26 and 2.28 mmol CO_2/g of the adsorbent were obtained, respectively.

The amine density of the sample with DG of 300% is about 15% higher than that of the sample with DG of 150%. It resulted in 14% higher adsorption capacity, indicating almost the same amine efficiency for two samples. However, for the sample with DG of 400%, even though the amine density is slightly higher than that of the sample with DG of 300%, the adsorption capacity and amine efficiency were lower, showing high pore blockage of the adsorbent and less access of CO_2

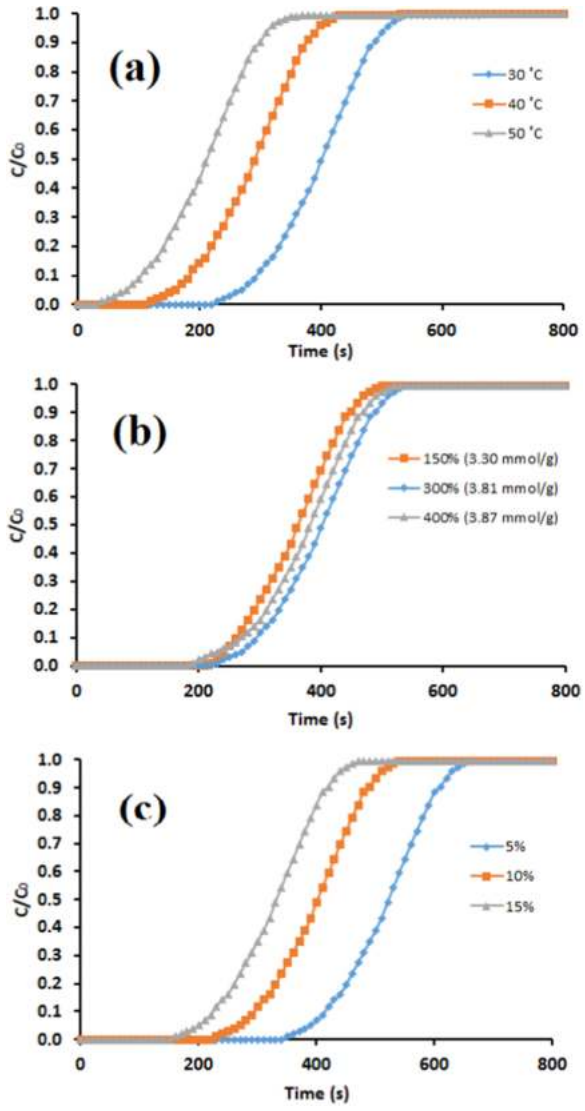

Fig. 7. Breakthrough curves for CO_2 adsorption at (a) different temperatures (C = 10%; DG = 300%; DA = 94%), (b) various DG/amine density (C = 10%; temperature = 30 °C), and (c) different feed concentration (DG = 300%; DA = 94%; temperature = 30 °C) for EA-aminated adsorbent.

Table 1
Comparison between the adsorption capacities of EA-aminated adsorbents.

T (°C)	C_0 (%)	DG (%)	DA (%)	Amine Density (mmol/g)	Amine Efficiency (%)	q (mmol/g)
30	10	300	94	3.81	67.5	2.57
40	10	300	94	3.81	43.8	1.67
50	10	300	94	3.81	27.3	1.04
30	10	150	98	3.30	68.5	2.26
30	10	400	90	3.87	59.0	2.28
30	5	300	94	3.81	49.8	1.90
30	15	300	94	3.81	75.3	2.87

molecules to amine functional groups.

Fig. 7C shows the effect of feed concentration on the breakthrough curve of CO_2 adsorption. As was expected, with an increase in the initial concentration of CO_2 in the feed, the breakthrough curve shifted to the left and the outlet concentration equaled to the inlet concentration at shorter times. So, at higher CO_2 concentrations, shorter times were required to reach the equilibrium point and the kinetics of the adsorption was faster. Moreover, the adsorption capacity and the amine efficiency also changed with the variation in the feed concentration. The increase in the feed concentration from 5% to 15% led to an increase in the amine efficiency from 49.8% to 75.3% and similar improvement in adsorption capacity from 1.90 to 2.87 mmol CO_2/g of the adsorbent.

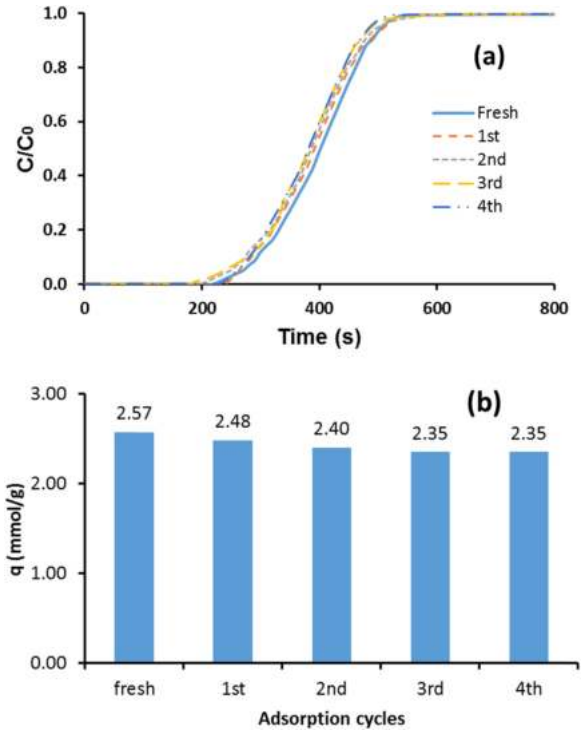

Fig. 8. Breakthrough curves of CO_2 adsorption on fresh and regenerated adsorbent (A) and CO_2 adsorption capacities (B) at each regeneration cycle (C = 10%; P = 1 bar and flow rate = 50 ml/min).

As can be seen in Table 1, the highest adsorption capacity among EA-aminated samples was 2.87 mmol/g, which was obtained for the adsorbent with DG of 300%, DA of 94% and CO_2 concentration of 15%. For all 7 samples used in this experiment, even though the adsorption capacity is moderate not high, but the amine efficiency is very high compared to other adsorbents (Zhuang et al., 2013; Mittal et al., 2015). With this amine efficiency, higher adsorption capacities are expected, but low amine density of the samples was the limiting parameter here. The s-PP part of the adsorbents as the carrier polymer contributed a large portion of the final weight of the samples without being involved in the adsorption process. Any modification in the material design that can decrease the inactive part of the adsorbent and increase the amine density will lead to a drastic increase in the adsorption capacity.

3.8. Regeneration

Regeneration performance of adsorbents is very important for practical applications. Fig. 8 shows the breakthrough curves (a) and CO_2 adsorption capacities (b) on fresh and regenerated samples at each regeneration cycle for the sample with 300% DG. As can be seen, the breakthrough curves of the fresh and regenerated samples are almost the same, indicating good stability of the adsorbent against regeneration process. The main decrease in the adsorption capacity was during the first and second regeneration cycles, leading to a 7% drop in the adsorption capacity from 2.57 to 2.40 mmol/g. after that, the capacity remained almost constant at 2.35 mmol/g for 2 more regeneration cycles.

Table 2
CO_2 adsorption properties of EA-aminated adsorbent in comparison with other amine functionalized solid sorbents.

Substrate	Amine group	Amine Efficiency (%)	Temp (°C)	q (mmol/g)	Regeneration temperature (°C)/time (min)	Refs.
PP nanofibers	**EA**	**75.3**	**30**	**2.87**	**80/15**	**This study**
Polyamide-6/CNT nanofibers	PEI	–	25	1.16	105/40	(Zainab et al., 2017)
SBA-15	Aziridine	44	25	3.11	130/180	(Hicks et al., 2008)
Glass microfibers	PEI	54	30	4.1	120/30	(Li et al., 2008)
Ion exchange resin	Benzyl amine	–	30	1.8	120/30	(Alesi and Kitchin, 2012)
Nanofibrillated cellulose	AEAPDMS	28	25	1.39	90/60	(Gebald et al., 2011)
Cellulose acetate hollow fibers	Aminosilane	–	35	0.23	–	(Li et al., 2013)
PAN microfibers	Allylamine	–	22	6.2	100/30	(Yang et al., 2010)
PP microfibers	TETA	46	30	4.72	100/20	(Zhuang et al., 2013)
PMMA	PEI	–	45	3.53	105/—	(Gray et al., 2009)

3.9. Comparison of developed adsorbent with previous studies

Comparison of adsorption related characteristics of developed adsorbents with some of the similar adsorbents reported in the literature was performed, as shown in Table 2. From the view point of adsorption capacity, the capacity of the new adsorbent is in the middle range, compared to other aminated adsorbents. For example, PP microfibers functionalized using triethylenetetramine (TETA) demonstrate an adsorption capacity of 4.72 mmol/g. This could be attributed to the use of tetramine molecule, having four amine functional groups per each amine molecule attached to the base PP backbone. This high number of amine functional groups increases the amine content of the adsorbent, leading to higher adsorption capacity.

Even though the adsorption capacity of EA-aminated nanofibrous adsorbent places this material in the group of middle-range CO_2 adsorbents, its amine efficiency of more than 75% is very high compared to other adsorbents. This could be originated from the high surface area of nanofibers and wider access of CO_2 molecules to amine groups. Another reason for middle CO_2 adsorption capacity in the present study is the use of mono-amine molecule in the functionalization stage, limiting the capacity of the adsorbent. Using di-, tri-, and tetramines could increase the adsorption capacity considerably. Another important characteristic of CO_2 adsorbents is regeneration energy. As could be seen in Table 2, most of the previously studied adsorbents were regenerated using temperatures between 100 and 130 °C for 30–130 min. However, the newly synthesized nanofibrous adsorbent was regenerated at 80 °C for 15 min which is lower than other materials. This decreases the energy required for the regeneration process and makes it more competitive with liquid amine absorption process. Also, lower regeneration temperature results in less structural degradation of the adsorbent and its longer life time. Stability of this new material is good after 4 times regeneration.

4. Conclusions

A new amine-bearing nanofibrous adsorbent for removal of CO_2 at ambient conditions was developed. The adsorbent was prepared in 3 consecutive stages involving electrospinning of s-PP, RIG of GMA, and amination with EA. The obtained s-PP nanofibers have average fiber diameters of 439 ± 173 nm and specific surface area of above 2 m^2/g. The average fiber diameter was increased by grafting of GMA and subsequent amination with EA. Various grafting parameters including time, temperature, absorbed dose and monomer concentration were found to have considerable effect on the DG. Moreover, the DA was heavily affected by amination parameters including amine concentration, reaction temperature, time and DG. A maximum DA of 98% was obtained for the sample with DG of 150% at 60 °C with 60% amine concentration in water medium in 120 min. The results of SEM, FTIR, DSC and TGA confirmed successful grafting and amination reactions. Also, the adsorbent showed reasonable mechanical characteristics with tensile strength of 18 ± 2 MPa and elongation at break of 53 ± 5%, making it more suitable for practical applications. The highest CO_2 adsorption capacity of 2.87 mmol/g was achieved for the sample with DG of 300%, DA of 94% and feed concentration of 15% at 30 °C. Even though the adsorption capacity is not high because of low amine density of the samples, high amine efficiency of 75% suggests a strong potential for the aminated nanofibrous structure to be used as adsorbent for CO_2. Furthermore, regeneration tests at relatively low temperature of 80 °C revealed low energy requirement for regeneration process and their good stability in 4 regeneration cycles.

Acknowledgment

This research was supported by Rachadapisek Sompote Fund for Postdoctoral Fellowship, Chulalongkorn University.

Appendix A. Supporting information

Supplementary data associated with this article can be found in the online version at doi:10.1016/j.radphyschem.2018.10.015.

References

Abbasi, A., et al., 2014. Electrospinning of nylon-6, 6 solutions into nanofibers: rheology and morphology relationships. Chin. J. Polym. Sci. 32 (6), 793–804.
Abbasi, A., et al., 2018. Highly flexible method for fabrication of poly (Glycidyl Methacrylate) grafted polyolefin nanofiber. Radiat. Phys. Chem. 151, 283–291.
Abouzari-lotf, E., et al., 2017. Phase separated nanofibrous anion exchange membranes with polycationic side chains. J. Mater. Chem. A.
Alesi, W.R., Kitchin, J.R., 2012. Evaluation of a primary amine-functionalized ion-exchange resin for CO_2 capture. Ind. Eng. Chem. Res. 51 (19), 6907–6915.
Almasian, A., et al., 2016. Surface modification of electrospun PAN nanofibers by amine compounds for adsorption of anionic dyes. Desalin. Water Treat. 57 (22), 10333–10348.
Bondar, Y., et al., 2004. Synthesis of cation-exchange adsorbent for anchoring metal ions by modification of poly(glycidyl methacrylate) chains grafted onto polypropylene fabric. React. Funct. Polym. 58 (1), 43–51.
Choi, S.H., Lee, K.P., Nho, Y.C., 2001. Adsorption of urokinase by polypropylene films with various amine groups. J. Appl. Polym. Sci. 80 (14), 2851–2858.
Choi, S.-H., Nho, Y., 1999. Adsorption of Pb2+, Cu2+ and Co2+ by polypropylene fabric and polyethylene hollow fiber modified by radiation-induced graft copolymerization. Korean J. Chem. Eng. 16 (2), 241–247.
Choi, S.-H., Nho, Y.C., Kim, G.-T., 1999. Adsorption of Pb2+ and Pd2+ on polyethylene membrane with amino group modified by radiation-induced graft copolymerization. J. Appl. Polym. Sci. 71 (4), 643–650.
Costa, L., et al., 2017. Template-synthesis of conjugated poly(3-hexylselenophene) (P3HS) nanofibers using femtosecond laser machined fused silica templates. MRS Adv. 2 (51), 2957–2960.
Drese, J.H., 2010. The Design, Synthesis, and Characterization of Aminosilica Adsorbents for CO_2 Capture from Dilute Sources. Georgia Institute of Technology, Atlanta, Ga.
Gebald, C., et al., 2011. Amine-based nanofibrillated cellulose As adsorbent for CO_2 capture from air. Environ. Sci. Technol. 45 (20), 9101–9108.
Gray, M.L., et al., 2009. Parametric study of solid amine sorbents for the capture of carbon dioxide. Energy Fuels 23 (10), 4840–4844.
Hicks, J.C., et al., 2008. Designing adsorbents for CO_2 capture from flue gas-hyperbranched aminosilicas capable of capturing CO_2 reversibly. J. Am. Chem. Soc. 130 (10), 2902–2903.
Hosseini, S., et al., 2015. CO_2 adsorption on modified carbon coated monolith: effect of surface modification by using alkaline solutions. Appl. Surf. Sci. 324 (0), 569–575.
IEA, 2015. CO_2 Emissions from Fuel Combustion: Highlights. International Energy Agency, Paris, pp. 152.
Kuenemann, M.A., Fourches, D., 2017. Cheminformatics modeling of amine solutions for

assessing their CO_2 absorption properties. Mol. Inform. 36 (7), 1600143.
Li, F.S., et al., 2013. Aminosilane-functionalized hollow fiber sorbents for post-combustion CO_2 capture. Ind. Eng. Chem. Res. 52 (26), 8928–8935.
Li, P.Y., et al., 2008. CO_2 capture by polyethylenimine-modified fibrous adsorbent. Langmuir 24 (13), 6567–6574.
Mittal, N., et al., 2015. Postcombustion CO_2 capture using N-(3-trimethoxysilylpropyl) diethylenetriamine-grafted solid adsorbent. Energy Sci. Eng. 3 (3), 207–220.
Nasef, M.M., et al., 2016. Radiation grafted adsorbents for newly emerging environmental applications. Radiat. Phys. Chem. 118, 55–60.
Nasef, M.M., Hegazy, E.S.A., 2004. Preparation and applications of ion exchange membranes by radiation-induced graft copolymerization of polar monomers onto non-polar films. Progress. Polym. Sci. 29 (6), 499–561.
Nasef, M.M., Abbasi, A., Ting, T.M., 2014. New CO_2 adsorbent containing aminated poly (glycidyl methacrylate) grafted onto irradiated PE-PP nonwoven sheet. Radiat. Phys. Chem. 103 (0), 72–74.
Olivieri, L., et al., 2018. Evaluation of electrospun nanofibrous mats as materials for CO_2 capture: a feasibility study on functionalized poly(acrylonitrile) (PAN). J. Membr. Sci. 546, 128–138.
Parvazinia, M., Garcia, S., Maroto-Valer, M., 2018. CO_2 capture by ion exchange resins as amine functionalised adsorbents. Chem. Eng. J. 331, 335–342.
Rochelle, G.T., 2009. Amine scrubbing for CO_2 capture. Science 325 (5948), 1652–1654.
Rojek, T., et al., 2017. Polyvinylamine-containing adsorbent by radiation-induced grafting of N-vinylformamide onto ultrahigh molecular weight polyethylene films and hydrolysis for CO_2 capture. Ind. Eng. Chem. Res. 56 (20), 5925–5934.
Serna-Guerrero, R., Sayari, A., 2010. Modeling adsorption of CO_2 on amine-functionalized mesoporous silica. 2: kinetics and breakthrough curves. Chem. Eng. J. 161 (1–2), 182–190.
Wahiduz, Zaman, et al., 2015. Fabrication of Polyacrylonitrile Nanofiber Membranes Functionalized With Metal Organic Framework for CO2 Capturing, 57526, p. V009T12A071.
Yang, Y., et al., 2010. Preparation and characterization of a solid amine adsorbent for capturing CO_2 by grafting allylamine onto PAN fiber. Langmuir 26 (17), 13897–13902.
Zainab, G., et al., 2017. Free-standing, spider-web-like polyamide/carbon nanotube composite nanofibrous membrane impregnated with polyethyleneimine for CO_2 capture. Compos. Commun. 6, 41–47.
Zhang, X.-F., et al., 2017. Temperature-induced formation of cellulose nanofiber film with remarkably high gas separation performance. Cellulose 24 (12), 5649–5656.
Zhuang, L., et al., 2013. Preparation of a solid amine adsorbent based on polypropylene fiber and its performance for CO_2 capture. J. Mater. Res. 28 (20), 2881–2889.